A cloud-scale lightning data assimilation technique implemented within the WRF-ARW model.

Alexandre O. Fierro[1], Edward R. Mansell[2], Conrad L. Ziegler[2]. Donald R. MacGorman[2] and Scott Dembek[1]
[1]Cooperative Institute for Mesoscale Meteorological Studies, Norman, Oklahoma, USA.
email: afierro@ou.edu, scott.r.dembek@nasa.gov
[2]National Severe Storms Laboratory/NOAA/OAR, Norman, Oklahoma USA,
email: Ted.Mansell@noaa.gov, Conrad.Ziegler@noaa.gov, Don.MacGorman@noaa.gov

ABSTRACT: To improve forecasts of convection, a new technique for assimilating total lightning data into the WRF-ARW model at cloud-resolving scales has been developed and evaluated over a large number of thunderstorm days. Assimilated lightning data forces deep, moist precipitating convection to occur via a nudging function for the total lightning data. This computationally inexpensive, smooth continuous function locally increases the water vapor mixing ratio and virtual buoyancy within the graupel-rich mixed phase region of storms at observed lightning locations. The assimilation of gridded pseudo-GOES-R resolution (9 km) flash rate via EarthNetworks® total lightning data for only a few hours prior to the forecast initialization significantly improved the representation of the convection at the initial analysis time and during the subsequent 1-3 forecast hours within the convection-permitting (≤ 5 km) and-resolving (≤ 2 km) grids. This lightning assimilation algorithm was also evaluated against a standard cloud-scale 3DVAR technique for the case of the 29 June 2012 "super derecho" event with this study emphasizing how the latter results can be extended to nocturnal outflow dominated mesoscale convective systems in general.

INTRODUCTION AND METHODOLOGY

Severe weather events are responsible for hundreds of fatalities and billions of dollars of damage annually in the United States alone. Therefore, there is considerable motivation to improve forecast skill for those events currently resolved by state-of-the-art numerical weather prediction (NWP) models. Toward this goal, it is proposed in the present work to assimilate total lightning data to provide an improved representation of the convection at the beginning of the forecasting period (i.e., analysis time). The rationale for conducting this modeling exercise arises from the existing well-known relationship between the occurrence of significant total lightning activity and deep convective updrafts and precipitation (e.g., MacGorman et al. 1989; Goodman et al. 1988; Wiens et al. 2005; Fierro et al. 2006), which allows for the development of lightning proxies within the aforementioned NWP models.

Only a limited number of studies, however, have attempted to assimilate lightning into forecast models. The first study from Alexander et al. (1999) demonstrated an improvement of 12-24 h rainfall forecast when lightning data were assimilated into an extra-tropical cyclone. Similar results were found a few years later by Chang et al. (2001). A preliminary operational application of lightning data is the inclusion of rain rates as a proxy for lightning in the model's initial conditions of the Rapid Update Cycle (RUC) model (Benjamin et al. 2004). Mansell et al. (2007) made use of the lightning data from the Oklahoma Lightning Mapping Array (LMA, Rison et al. 1999, MacGorman et al. 2008) and the National Lightning Detection Network (NLDN, Cummins and Murphy 2009; Biagi et al. 2007) by modifying the Kain-Fritsch convective parameterization scheme (CPS) to allow the lightning data to control the 'trigger' function within this CPS scheme. Pessi and Businger (2009) assimilated Pacific Lightning Detection Network (PacNet/LLNN) lightning data by adjusting the latent heating profile produced by the CPS for a

Pacific storm case. Papadopoulos et al. (2005) utilized real-time CG flash-rate data from a long-range lightning detection network to force deep moist convection into a regional mesoscale model by nudging the simulated humidity profiles to empirical profiles representative of convective regimes from observed soundings during thunderstorm days. None of the aforementioned works, however, conducted assimilation of total lightning data at cloud resolving scales (i.e., $\Delta x \leq 3$ km), the latter objective being emphasized by the present study.

The numerical model used for assimilation is WRF-ARW (version 3). In developing our assimilation technique, the choice of the physics parameterizations and large-scale fields necessary for providing the initial and boundary conditions were inspired by the National Severe Storms Laboratory (NSSL) daily forecast runs over the contiguous United States (CONUS) (Kain et al. 2011). The initial and boundary conditions were derived from the 6-hourly North American Mesoscale Model (NAM) 40-km and 12 km reanalysis and forecast data made publicly available by NCDC/NCEP.

The ENTLN point flash data were gridded from their latitude and longitude coordinates onto the local WRF Cartesian grid coordinates and accumulated over 10-min intervals to resolve storm movement during the assimilation period (usually 2-3 h). For the case of the 24 May 2011 Oklahoma tornado outbreak, the lightning data was first interpolated onto the 9-km resolution parent domain and then projected onto the inner nests by simply assigned the value of the flash rate within a given 9 x 9 km^2 grid cell onto all the finer-resolution grid cells encompassed within it. The motivation for this procedure is twofold: (i) the assimilation assumes a future scenario in which GLM resolution (i.e., 8-12 km) lightning data are readily available and (ii) using identical lightning fields (gridded flash rate) and lightning areal coverage for all grids allows an equal amount of nudging to be performed on all three grids.

The parsed lightning data was assimilated into the WRF microphysics using the following procedure (described in detail in Fierro et al. 2012): Whenever a flash occurs in a given grid column, water vapor is added at constant temperature to the graupel-rich, "mixed-phase" region in that column (defined as the layer between the 0° and -20°C isotherms). This is the layer most likely associated with the dominant electrification mechanism via noninductive graupel-ice interactions (e.g., Saunders and Peck 1998). The water vapor (Q_v) addition is performed via a smooth continuous function with gridded flash rate (X) and the simulated graupel mixing ratio (Q_g) as the main input variables:

$$Q_v = AQ_{sat} + BQ_{sat} \tanh(CX) [1 - \tanh(DQ_g^a)],$$

where Q_{sat} is the water vapor saturation mixing ratio (g kg^{-1}). With hyperbolic tangent functions it becomes relatively easy to determine the slope (via C and D) and the asymptotic value of the function (via B and A). The values of these four constants in Fierro et al. (2012) revealed being optimal over a wide range of convective regimes (Fig. 1). The local increase in water vapor [and hence relative humidity (RH)] is applied only if the RH at the time step within the corresponding grid point in the mixed-phase region is below a fixed threshold (set to 80% for May 24 2011 and 90% for 29 June 2012) and below a fixed Q_g value (set to 3 g kg^{-1} for both days). Thus, nudging of Q_v is reduced or not applied if the grid point already has conditions favorable for updraft development (RH>80%) or already has or lies within a convective cloud (as indicated by Q_g).

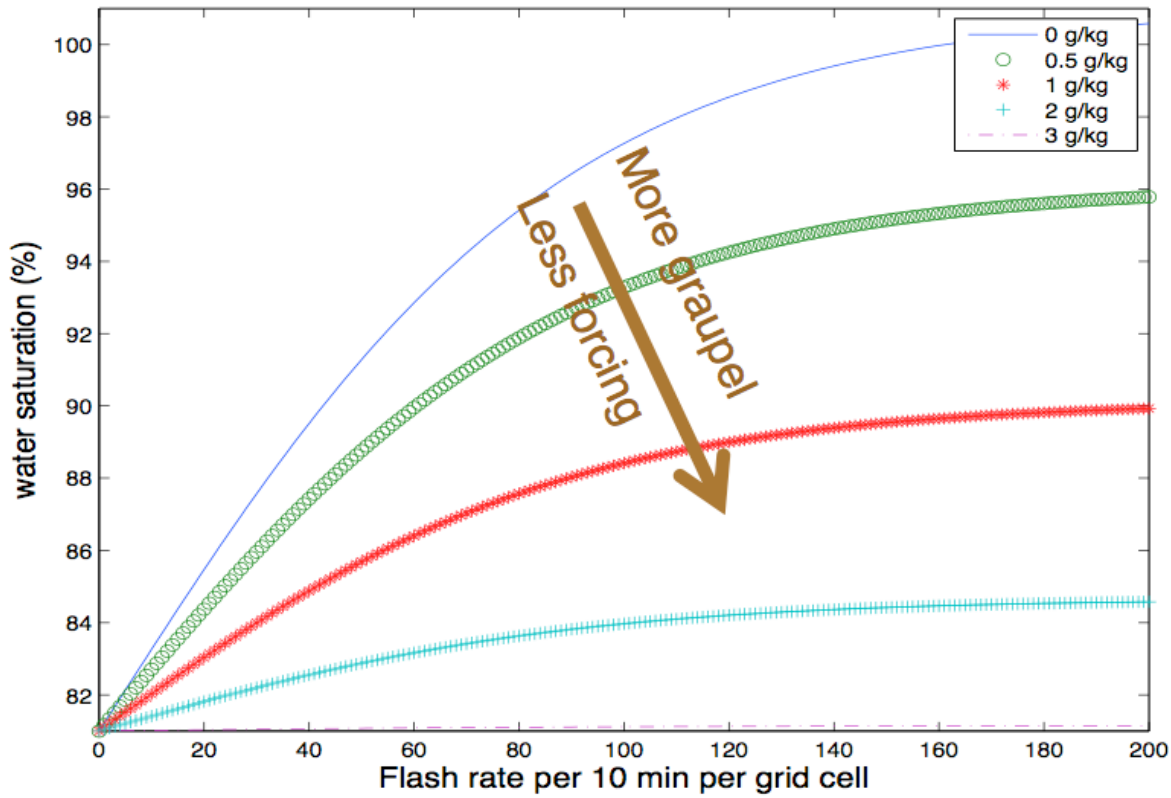

Figure 1. Plot of the water vapor nudging function for several values of graupel mixing ratios in g kg^{-1} with legend shown on the top right corner of the figure. Figure adapted from Fierro et al. (2012)

While in the two cases shown herein employ the WSM6 microphysics, this lightning assimilation scheme has been coded as a stand-alone FORTRAN module, allowing (i) the assimilation to be performed/tested with any microphysics scheme available in WRF and (ii) a relatively easy/smooth implementation into other versions of WRF.

1. RESULTS

Results from this procedure for two high impact weather case studies are presented in Fierro et al. (2012, 2014), and are summarized here.

In the first study (Fierro et al. 2012), the simulation domain contained two nested grids with horizontal spacing of 3 km and 1 km (the parent domain had 9 km horizontal grid spacing) and employed ENTLN data as proxy for GLM data. These grid spacings were intentionally selected to be representative of convection-resolving (1 km) and convection-allowing (3 km) scales, as used in several experimental NWP models, and of the scheduled GLM resolution over CONUS (9 km).

For the case of the Oklahoma tornado outbreak of 24 May 2011, Figure 2 shows clearly that the lightning assimilation results in a much improved representation of the convection at the analysis time and at the 1-hour forecast with the assimilation starting to show already some noticeable improvements of near-surface precipitation at 1-hour into the assimilation. The improvements in the reflectivity field are best seen in north-central OK and to some degree in northern TX. While the assimilation of total lightning data clearly aids the model in forcing the convection at the right place, the assimilation does not prevent the development of spurious convection as indicated by a second cold pool in central OK (not shown). This suggests that especially for case studies where thermodynamic conditions for strong convection are

widespread, (e.g., low CIN below ~20 J kg^{-1} and moderate CAPE magnitudes in excess of ~1500 J kg^{-1}), assimilating total lightning data might not have notable desired effects unless the spurious convection is limited during the lightning assimilation period.

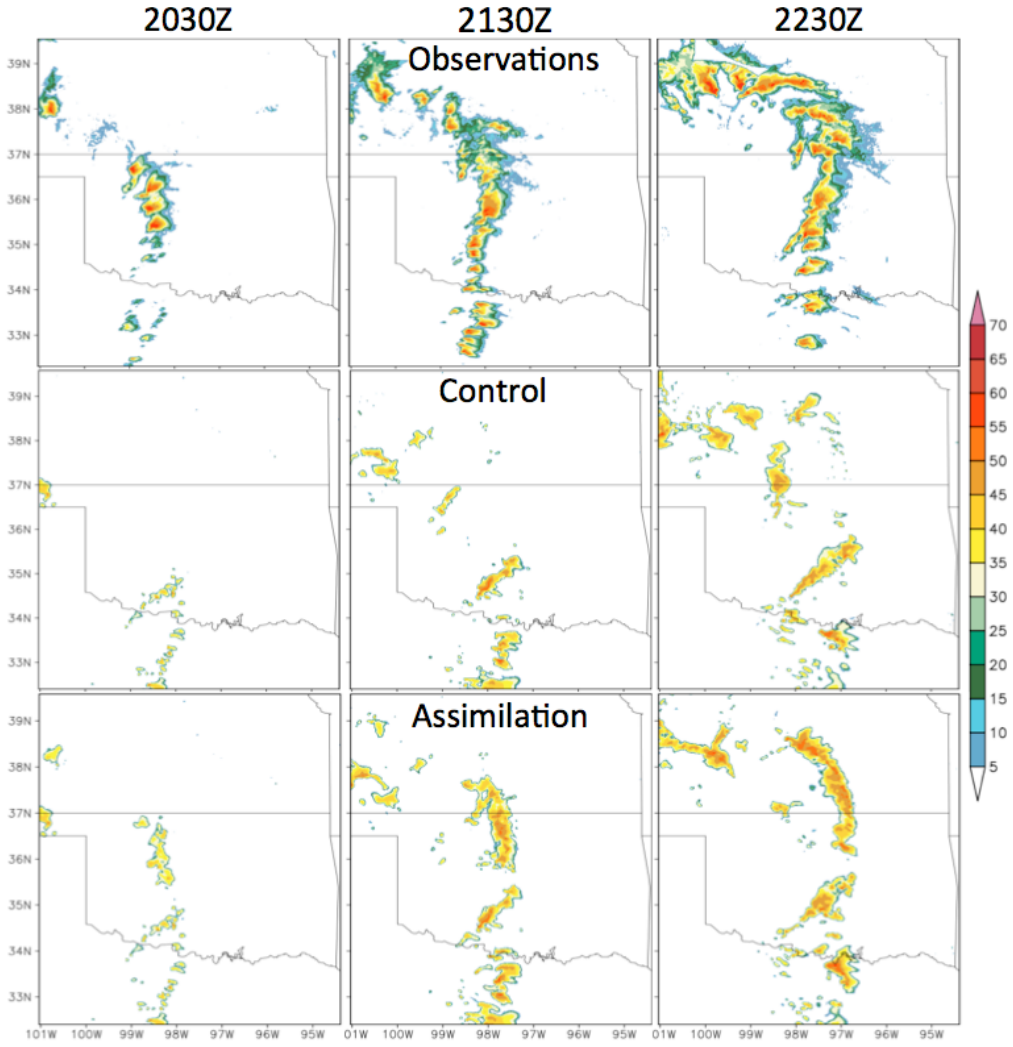

Figure 2. The first row shows interpolated radar reflectivity from the NM2Q product onto the 3 km (D02) grid using the same domain boundaries as the finest resolution grid (1-km = D03). The three times shown 2030 UTC (during assimilation period), 2130 UTC (end of assimilation period or analysis time) and 2230 UTC (1-h forecast). The second (middle) row simulated radar reflectivity (in dBZ) for the CTRL run and the last row shows simulated reflectivity fields for the lightning assimilation run. Legends for shadings of all panes are shown on the right of the figure. Figure adapted from Fierro et al. (2012).

For the second case study presented here, namely the "super derecho" of 29 June 2012, the simulation domain (Fig. 3) has a uniform horizontal grid spacing of 3 km and horizontal dimensions in grid points of (1001 x 501). The stretched vertical grid has 35 levels with model top set at 50 hPa (~20 km). The initial and time-dependent lateral boundary conditions employ the 6-hourly, 12-km NAM operational analysis data for a 18-h period starting at 1200 on 29 June 2012. The computational time step is set to 15 s and the lightning data was, as before, parsed into 10 min intervals to resolve storm movement and interpolated onto the local WRF 3-km grid.

The 3DVAR assimilation procedure (Gao and Stensrud 2012) makes use of standard WSR-88D Level II data. For this study, radar reflectivity and radial velocity data from six radar sites have been employed (Fierro et al. 2014, their Fig. 3). The rationale behind the choice of these particular radar sites is to reasonably capture the development of the embryonic thunderstorm clusters in eastern Iowa and northern Illinois that is well advanced by 1600. For consistency, the 3DVAR assimilation is performed during the same 2-h period as the ENTLN lightning assimilation. Owing to the computational expense dictated by the relatively large model grid used herein (~1.8x107 grid cells) the frequency of the 3DVAR cycles is set to 30 min.

When neither lightning nor radar data are assimilated (CTRL), the model fails to initiate convection at 1600 in eastern Iowa and northern Illinois (Fig. 3a vs. Fig. 3d). Instead, CTRL develops a thunderstorm cluster near the observed location of the embryonic MCS-derecho 3 h later in the simulation (Fig. 3b vs. Fig. 3e) that moves east-southeastward with other, later storms that develop ahead of its leading edge in southern Ohio (Fig. 3c vs. Fig. 3f). Both LIGHT (Figs. 3a-c vs. Figs. 3g-i) and ALL (Figs. 3a-c vs. Figs. 3j-l) clearly outperformed CTRL. In the 3-h and 6-h forecasts, the MCS produced by LIGHT (Figs. 3h-i) is in better agreement with observations (Figs. 3b-c) than the ALL-generated MCS (Figs. 3k-l). A spurious cluster of thunderstorms is produced by ALL ahead of the intensifying parent MCS beginning around 1700-1800 (i.e., 1-2 h into the forecast), as evidenced by unobserved convection over southeastern Indiana (not shown). The spurious convection over Indiana subsequently leads to the early demise of the parent MCS (compare Figs. 3h and 3k). Eventually, the spurious thunderstorm cluster forms a new convective system ahead of the original MCS before intensifying and moving east-southeastward (compare Figs. 3i and 3l vs. Fig. 3c). This spurious discrete propagation episode explains why the ALL-simulated MCS is further displaced to the east compared to the LIGHT-simulated MCS at the 6-h forecast time (compare Figs. 3i and 3l).

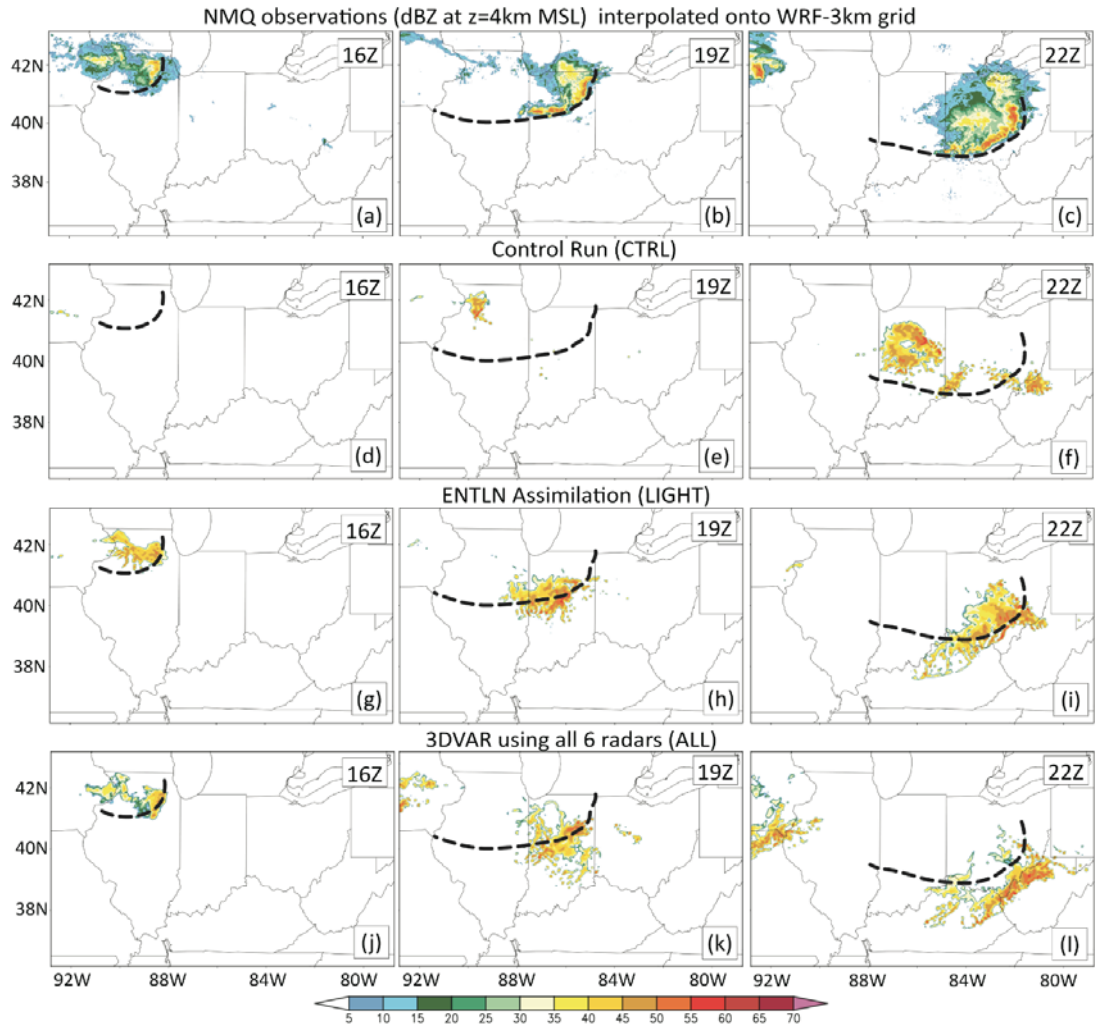

Figure 3. Observed and modeled reflectivity fields (dBZ) at 4 km AGL. The top row shows observed reflectivity fields at z=4km MSL from the NM2Q product at (a) 1600, (b) 1900 and (c) 2200 UTC June 29 2012. The second row (d-f) shows results from the control simulation (CTRL). The third row (g-i) is as in (d-f) but for the lightning assimilation run (LIGHT). The bottom row (j-l) is as (g-i) but for the 3DVAR assimilation run using all 6 radars (ALL) in Fig. 3. The thick black dashed curves denote the positions of the leading edge of the cold pool boundary as inferred from clear-air NSSL mosaic reflectivity fields. Legends for colors and shadings are shown on the bottom of the figure. Figure adapted from Fierro et al. (2014).

As indicated by the inferred location of the leading edge of the outflow boundary (Fig. 3), at 3-h (6-h) the LIGHT-simulated MCS forecast exhibits a noteworthy southward (southeastward) displacement from the observations. One potential factor for this disparity might be the overestimation of evaporation rates in the sub-cloud layer of the MCS produced by the WSM6 microphysics which would force an overly-intense mesoscale cold pool and density current propagating too quickly against the ambient southwesterly surface winds (e.g., Ziegler et al. 2010). The overall lack of stratiform region in the simulated MCS is also noted. A possible cause of too little stratiform precipitation area is the inability of single moment schemes to accurately simulate transitions from regions of high concentration of small particles to relatively low concentrations of larger particles associated with ice growth via deposition, aggregation, and riming or, as mentioned in Fierro et al. (2012), that neither

low-density graupel nor aggregate are well represented in single-moment schemes.

The presence of the spurious thunderstorm cluster in southeastern Indiana ahead of the main MCS-derecho in ALL (Fig. 3k) is evident in the spurious cold-pool temperature perturbation (not shown).

Figure 4 shows simulation results for the 31 May 2013 tornado outbreak conducted in real-time during the WRF-NSSL 4-km testbed over CONUS (e.g., Kain et al. 2011). The fuzzy logic pattern recognition algorithm ('MET' Tool) highlights how the assimilation of lightning improves the 6-h accumulated precipitation (APCP) fields in Fig. 4 in the warm, convective, sector. The stratiform rainy areas in the northern plains remained unaltered as no lightning was detected by ENTLN.

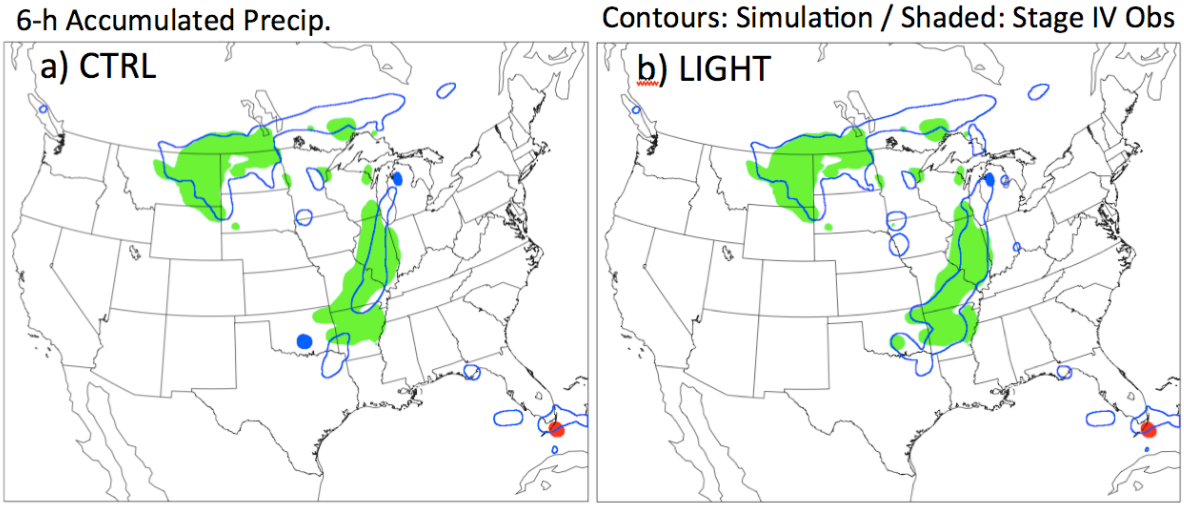

Figure 4. MODE Fuzzy Logic Object pattern recognition algorithm (MET tool) for the 6-h accumulated precipitation field for the case of the 31 May 2013 tornado outbreak. Blue contours show the forecast and shaded green/red contours indicate the corresponding stage IV multisensory rainfall estimates for (a) control run (CTRL) and (b) lightning assimilation run (LIGHT). The stage IV dataset is made publicly available courtesy of http://data.eol.ucar.edu.

Another representative example from last Spring highlighting the improvement of LIGHT is provided in Fig. 5 for the May 30 2013 MCSs case over the Nebraska-Kansas-Oklahoma. A side-by-side comparison between the last 10-min bin (0150-0200UTC) of the assimilated ENTLN data and the LIGHT APCP fields at 0200UTC, revealed a high spatial agreement (Figs. 5m and 5i) in contrast to CTRL (Figs. 5m and 5e). Although less evident, a similarly noteworthy spatial collocation is seen between the ENTLN fields and the OBS at 0200UTC (compare Figs 5m and 5a). Despite this good spatial agreement between LIGHT and OBS, the LIGHT APCP fields clearly are overestimated by almost an order of magnitude in some places (e.g., convection of Oklahoma, Figs. 5b and 5j). Note that CTRL also exhibits a tendency to overestimate APCP after the end of the spin up period at about 0200UTC (e. g., Figs. 5b and 5f). During the spin up period, however, the CTRL-simulated APCP generally are smaller than observed (< 20 mm, not shown).

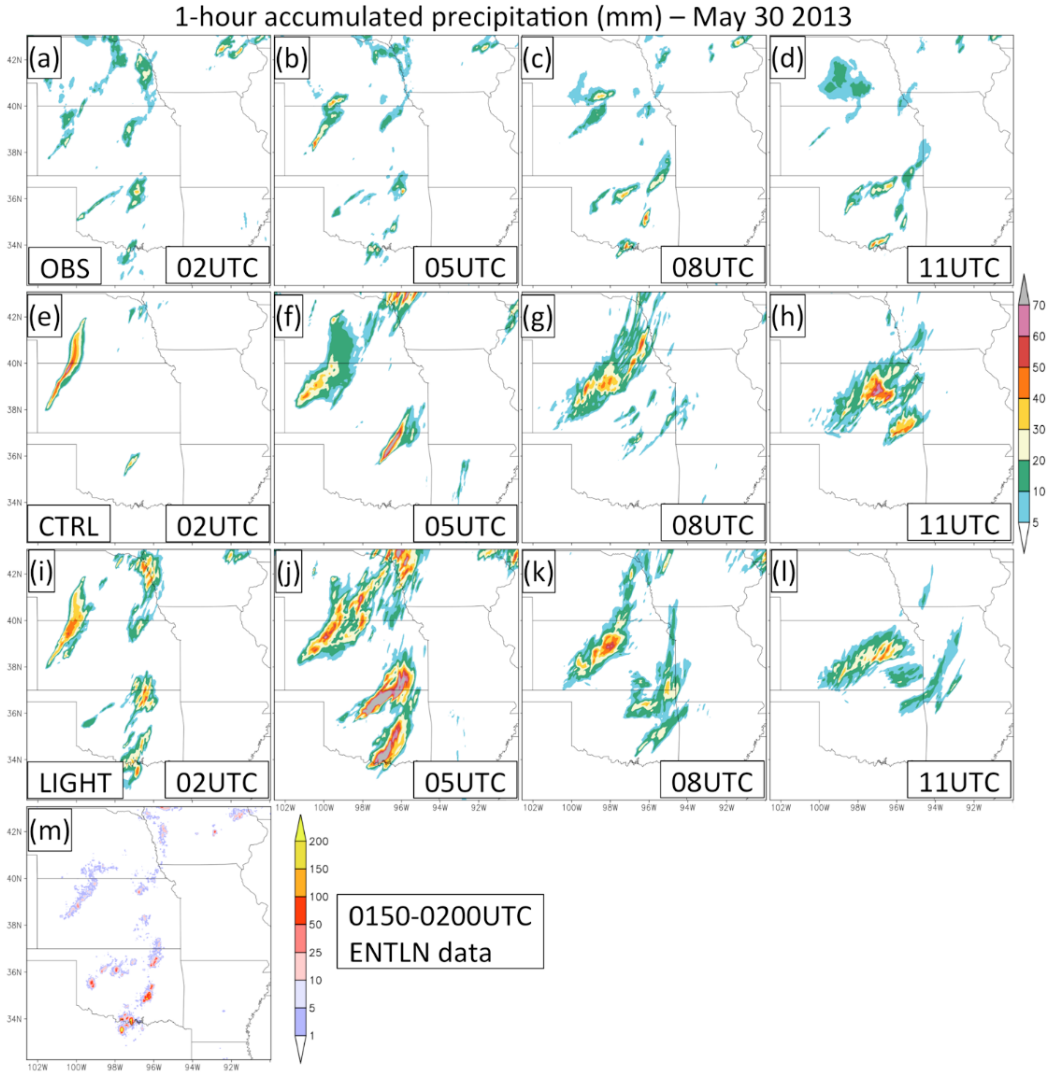

Figure 5. Horizontal cross sections of hourly APCP (ending at the time shown in the plot) zoomed over the Central Plains from the stage IV data interpolated onto the local 4-km D01 domain at (a) 0200, (b) 0500, (c) 0800 and (d) 1100UTC on 30 May 2013. The second row from (e)-(h) is as in (a)-(d) but for the CTRL run. (i)-(l) is as in (e)-(h) but for LIGHT. Finally, (m) shows the ENTLN data interpolated onto D01 for the last 10 min (bin) of assimilation from 0150-0200UTC.

A total of 67 cases with and without lightning assimilation (again, using ENTLN data) were simulated during the 2013 warm season (spanning the period from May to July) over CONUS using the 4-km WRF-NSSL testbed set up (Kain et al. 2011). As indicated by the positive differences in bias-corrected aggregate, equitable threat score values for different neighborhood (Clark et al. 2010) radii in Fig. 6, the simulations assimilating ENTLN lightning (LIGHT) shows a clear improvement in forecasted APCP relative to CTRL (cold start) for those 67 cases (Figs. 6 c, f, i). These improvements were seen for various APCP thresholds (i.e., ranging from 2.5 to 50 mm) and for 3h, 6h , 12h and 24h APCP, respectively (not shown). Figure 6 also highlights that the improvements in APCP is maintained up to ~12-h of simulation and are of similar magnitude of those reported when assimilating conventional radar data through more sophisticated assimilation (e.g., variational) techniques.

To determine the statistical significance of the ETS differences (between LIGHT and CTRL)

shown in Fig, 6, a bootstrapping re-sampling approach following Hamill (1999) was applied on the ETS differences for each of 67 cases and repeated 1000 times. The analysis revealed that for the 1h and 3h APCP, the ETS differences were essentially insignificant while for higher APCP partitioning (6, 12h and 24h), the differences in ETS were significant up to 12h of simulation. In all cases and that despite this noteworthy improvements from the assimilation of lightning data, the positive ETS (or fraction skill score, not shown) difference between LIGHT and CTRL decreased to near 0 (i.e., statistically insignificant) values past 9 to 12-h indicating that regardless of the method employed herein to initially place the convective features at the correct locations during the assimilation period, the inherent errors in the initial conditions will progressively force the solutions of LIGHT to converge to that of CTRL.

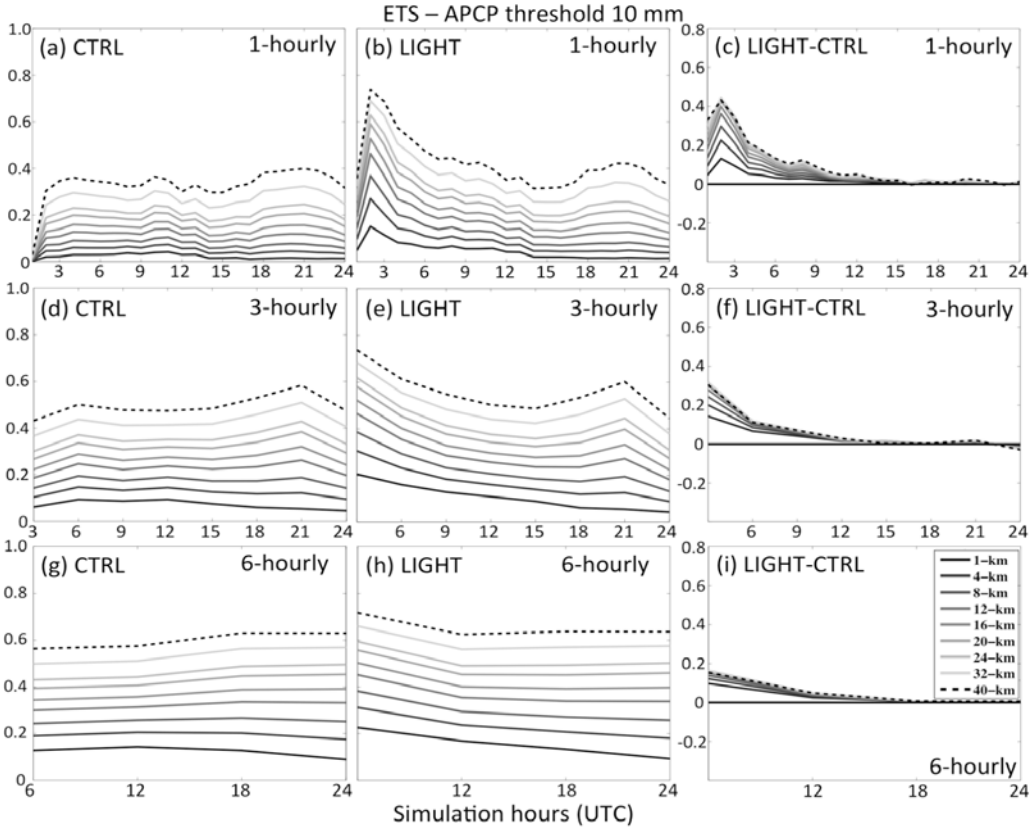

Figure 6. Bias-corrected aggregate ETS for the 1-h APCP threshold of 10 mm for (a) CTRL, (b) LIGHT and (c) the difference between LIGHT and CTRL. (d)-(f) are as in (a)-(c) but for 3-hourly APCP and, finally, (g)-(i) are as in (a)-(c) but for 6-hourly APCP. ETS are shown for all the nine neighborhood radii considered in this study, with the legend shown on the lower right corner of the figure.

2. FUTURE WORK AND CONCLUSIONS

Using WRF-ARW, a computationally inexpensive lightning nudging scheme was evaluated in detail for the forecast of the Oklahoma tornado outbreak of 24 May 2011 and the 29–30 June 2012 derecho case. For both cases, the overall radar reflectivity fields at analysis time were in better agreement with the observations than in the control case. Additionally, for 29 June, the subsequent 3- and 6-h forecasts showed better agreement with the radar reflectivity observations when total lightning data was assimilated than when utilizing a state-of-the art cloud-scale 3DVAR code. This improvement may be

attributed to a better representation of the mesoscale and convective-scale cold pools (e.g., Mansell et al. 2007) or the midtropospheric heating profiles and associated cell-scale circulations from the assimilation-induced convection (Fierro et al. 2012) at the analysis time.

Additional work is ongoing to focus on establishing meaningful statistics of the performance of the lightning assimilation scheme at the cloud scale (4km) over CONUS (Kain et al. 2010) during the course of the 2013 spring and early summer seasons (e.g., Fig. 6). The distribution of convection during the warm season may be expected to include many thunderstorm days and span various convective regimes including isolated storms, MCSs, and landfalling mesoscale tropical convective systems. Some recent preliminary results of convection- allowing model forecasts initialized at 0000 UTC during the 2013 warm season suggest that the lightning assimilation technique seems to perform best on days favorable for the development of nocturnal MCSs. The reasons for this behavior are threefold: (i) climatologically, nocturnal MCSs often initiate/form within the 0000–0200 UTC period when lightning data were assimilated; (ii) the large-scale environment is usually depicted well by the reanalysis (including the nocturnal low-level jet); and (iii) the upscale evolution and placement of MCSs are strongly dictated by the initial placement and intensity of convectively induced cold pools.

ACKNOWLEDGMENTS

Funding was provided by NOAA/ Office of Oceanic and Atmospheric Research under NOAA-University of Oklahoma Cooperative Agreement NA08OAR4320904, U.S. Department of Commerce. This work was supported by the NESDIS program, which is under the auspices of the National Oceanic and Atmospheric Administration of the U.S. Department of Commerce under Grant NOAA-NESDIS- OAR-NA08OAR4320904. Computer resources were provided both by the Oklahoma Supercomputing Center for Education and Research (OSCER) hosted at the University of Oklahoma. The authors thank Ami Arthur for providing the NSSL three-dimensional NMQ radar mosaic data. Thanks also go out to Steve Prinzivalli, Stan Heckman, and Jim Anderson from Earth Networks for providing the total lightning data.

REFERENCES

Alexander, G. D., J. A. Weinman, V. Karyampudi, W. S. Olson and A. C. L. Lee, 1999: The effect of assimilating rain rates derived from satellites and lightning on forecasts of the 1993 Superstorm. *Mon. Wea. Rev*., **127**, 1433–1457.

Benjamin, S. G., and Coauthors, 2004: An hourly assimilation–forecast cycle: The RUC. *Mon. Wea. Rev*., **132**, 495–518. doi: 10.1175/1520-0493(2004)132<0495:AHACTR>2.0.CO;2.

Biagi C. J., K. L. Cummins, K. E. Kehoe, E. P. Krider, 2007: National Lightning Detection Network (NLDN) performance in southern Arizona, Texas, and Oklahoma in 2003–2004, J. *Geophys. Res.*, **112**, D05208,doi:10.1029/2006JD007341.

Chang, D.-E, J. A. Weinman, C. A. Morales and W. S. Olson, 2001: The effect of spaceborne microwave and ground-based continuous lightning measurements on forecasts of the 1998 Groundhog Day storm. *Mon. Wea. Rev*., **129**, 1809–1833.

Clark, Adam J., William A. Gallus, Morris L. Weisman, 2010: Neighborhood-Based Verification of Precipitation Forecasts from Convection-Allowing NCAR WRF Model Simulations and the Operational NAM. *Wea. Forecasting*, **25**, 1495–1509.

Cummins, K. L. and M. J. Murphy, 2009: An overview of lightning location systems: History, techniques, and data uses, with an in-depth look at the U.S. NLDN, *IEEE Trans. Electromag. Compat.*, **51**, 499-518.

Fierro, A. O., M. S. Gilmore, E. R. Mansell, L. J. Wicker, J. M. Straka, 2006: Electrification and lightning in an idealized boundary-crossing supercell Simulation of 2 June 1995. *Mon. Wea. Rev*., **134**, 3149–3172.

Fierro, A. O., R. F. Rogers, F. D. Marks and D. S. Nolan, 2009: The impact of horizontal grid spacing on the microphysical and kinematic structures of strong tropical cyclones simulated with the WRF-ARW model. *Mon. Wea. Rev*., **137**, 3717–3743.

Fierro, A. O., and J. M. Reisner, 2011: High-resolution simulation of the electrification and lightning of

Hurricane Rita during the period of rapid intensification. *J. Atmos. Sci*., **68**, 477–494.

Fierro, A. O., E.R. Mansell, C. Ziegler and D. R. MacGorman 2012: Application of a lightning data assimilation technique in the WRF-ARW model at cloud-resolving scales for the Tornado Outbreak of 24 May 2011. *Monthly Weather Review*, Volume **140**, 2609-2627.

Fierro, A. O., J. Gao, C. Ziegler, E.R. Mansell, D. R. MacGorman and S. Dembek 2014: Evaluation of a cloud scale lightning data assimilation technique and a 3DVAR method for the analysis and short term forecast of the 29 June 2012 derecho event. *Monthly Weather Review*, Volume **142**, 183-202.

Gao, J., and D. J. Stensrud, 2012: Assimilation of reflectivity data in a convective-scale, cycled 3DVAR framework with hydro- meteor classification. J. Atmos. Sci., 69, 1054–1065.

Goodman, S. J., D. E. Buechler, P. D. Wright, and W. D. Rust, 1988: Lightning and precipitation history of a microburst-producing storm. *Geophys. Res. Lett.*, **15**, 1185–1188.

Hamill, Thomas M., 1999: Hypothesis Tests for Evaluating Numerical Precipitation Forecasts. Wea. Forecasting, 14, 155–167.

Kain, J. S., S. R. Dembeck, S. J. Weiss, J. L. Case, J. J. Levit, and R. A. Sobash, 2010: Extracting unique information from high- resolution forecast models: Monitoring selected fields and phenomena every time step. Wea. Forecasting, 25, 1536–1542.

MacGorman, D. R and Coauthors, 2008: TELEX: The Thunderstorm Electrification and Lightning Experiment. Bull. Amer. Meteor. Soc., 89, 997–1013.

MacGorman, D. R., D. W. Burgess, V. Mazur, W. D. Rust, W. L. Taylor and B. C. Johnson, 1989: Lightning rates relative to tornadic storm evolution on 22 May 1981. *J. Atmos. Sci*., **46**, 221–251.

MacGorman D. R. and W. D. Rust, 1998: The electrical nature of storms. Oxford: Oxford University Press. pp. 422.

Mansell, E. R., C. L. Ziegler, D. R. MacGorman, 2007: A lightning data assimilation technique for mesoscale forecast models. *Mon. Wea. Rev*., **135**, 1732–1748.

Papadopoulos, A., T. G. Chronis and E. N. Anagnostou, 2005: Improving Convective Precipitation Forecasting through Assimilation of Regional Lightning Measurements in a Mesoscale Model. *Mon. Wea. Rev.*, **133**, 1961–1977.

Pessi A. T, and S. Businger, 2009: The impact of lightning data assimilation on a winter storm simulation over the north Pacific ocean. *Mon. Wea. Rev.*, **137**, 3177-3195.

Rison W., Thomas R. J., Krehbiel P. R., Hamlin, and T. Harlin, 1999: J. A GPS-based three-dimensional lightning mapping system: Initial observations. *Geophys. Res. Lett*., **26**: 3573-3576.

Wiens, K. C., S. A. Rutledge, and S. A. Tessendorf, 2005: The 29 June 2000 supercell observed during STEPS. Part II: Lightning and charge structure. *J. Atmos. Sci*., **62**, 4151–4177.

Ziegler, C. L., E. R. Mansell, J. M. Straka, D. R. MacGorman and D. W. Burgess, 2010: The impact of spatial variations of low-level stability on the life cycle of a simulated supercell storm. *Mon. Wea. Rev*., **138**, 1738–1766.